

- ¹⁷University of California at Santa Cruz, Institute for Particle Physics, Santa Cruz, CA 95064, USA
¹⁸California Institute of Technology, Pasadena, CA 91125, USA
¹⁹University of Cincinnati, Cincinnati, OH 45221, USA
²⁰University of Colorado, Boulder, CO 80309, USA
²¹Colorado State University, Fort Collins, CO 80523, USA
²²Technische Universitat Dresden, Institut fur Kern- und Teilchenphysik, D-01062 Dresden, Germany
²³cole Polytechnique, LLR, F-91128 Palaiseau, France
²⁴University of Edinburgh, Edinburgh EH9 3JZ, United Kingdom
²⁵Universita di Ferrara, Dipartimento di Fisica and INFN, I-44100 Ferrara, Italy
²⁶Florida A & M University, Tallahassee, FL 32307, USA
²⁷Laboratori Nazionali di Frascati dell'INFN, I-00044 Frascati, Italy
²⁸Universita di Genova, Dipartimento di Fisica and INFN, I-16146 Genova, Italy
²⁹Harvard University, Cambridge, MA 02138, USA
³⁰Universitat Heidelberg, Philosophisches Institut, Philosophenweg 12, D-69120 Heidelberg, Germany
³¹Imperial College London, London, SW7 2AZ, United Kingdom
³²University of Iowa, Iowa City, IA 52242, USA
³³Iowa State University, Ames, IA 50011-3160, USA
³⁴Laboratoire de l'Accelerateur Linéaire, F-91898 Orsay, France
³⁵Lawrence Livermore National Laboratory, Livermore, CA 94550, USA
³⁶University of Liverpool, Liverpool L69 7ZE, United Kingdom
³⁷Queen Mary, University of London, E1 4NS, United Kingdom
³⁸University of London, Royal Holloway and Bedford New College, Egham, Surrey TW20 0EX, United Kingdom
³⁹University of Louisville, Louisville, KY 40292, USA
⁴⁰University of Manchester, Manchester M13 9PL, United Kingdom
⁴¹University of Maryland, College Park, MD 20742, USA
⁴²University of Massachusetts, Amherst, MA 01003, USA
⁴³Massachusetts Institute of Technology, Laboratory for Nuclear Science, Cambridge, MA 02139, USA
⁴⁴McGill University, Montreal, QC, Canada H3A 2T8
⁴⁵Universita di Milano, Dipartimento di Fisica and INFN, I-20133 Milano, Italy
⁴⁶University of Mississippi, University, MS 38677, USA
⁴⁷Universite de Montreal, Laboratoire Rene J. A. Levesque, Montreal, QC, Canada H3C 3J7
⁴⁸Mount Holyoke College, South Hadley, MA 01075, USA
⁴⁹Universita di Napoli Federico II, Dipartimento di Scienze Fisiche and INFN, I-80126, Napoli, Italy
⁵⁰NIKHEF, National Institute for Nuclear Physics and High Energy Physics, NL-1009 DB Amsterdam, The Netherlands
⁵¹University of Notre Dame, Notre Dame, IN 46556, USA
⁵²Oak Ridge National Laboratory, Oak Ridge, TN 37831, USA
⁵³Ohio State University, Columbus, OH 43210, USA
⁵⁴University of Oregon, Eugene, OR 97403, USA
⁵⁵Universita di Padova, Dipartimento di Fisica and INFN, I-35131 Padova, Italy
⁵⁶Universites Paris VI et VII, Laboratoire de Physique Nucléaire et de Hautes Energies, F-75252 Paris, France
⁵⁷Universita di Pavia, Dipartimento di Elettronica and INFN, I-27100 Pavia, Italy
⁵⁸University of Pennsylvania, Philadelphia, PA 19104, USA
⁵⁹Universita di Perugia, Dipartimento di Fisica and INFN, I-06100 Perugia, Italy
⁶⁰Universita di Pisa, Dipartimento di Fisica, Scuola Normale Superiore and INFN, I-56127 Pisa, Italy
⁶¹Prairie View A & M University, Prairie View, TX 77446, USA
⁶²Princeton University, Princeton, NJ 08544, USA
⁶³Universita di Roma La Sapienza, Dipartimento di Fisica and INFN, I-00185 Roma, Italy
⁶⁴Universitat Rostock, D-18051 Rostock, Germany
⁶⁵Rutherford Appleton Laboratory, Chilton, Didcot, Oxon, OX11 0QX, United Kingdom
⁶⁶DSM /Dapnia, CEA/Saclay, F-91191 Gif-sur-Yvette, France
⁶⁷University of South Carolina, Columbia, SC 29208, USA
⁶⁸Stanford Linear Accelerator Center, Stanford, CA 94309, USA
⁶⁹Stanford University, Stanford, CA 94305-4060, USA
⁷⁰State Univ. of New York, Albany, NY 12222, USA
⁷¹University of Tennessee, Knoxville, TN 37996, USA
⁷²University of Texas at Austin, Austin, TX 78712, USA
⁷³University of Texas at Dallas, Richardson, TX 75083, USA
⁷⁴Universita di Torino, Dipartimento di Fisica Sperimentale and INFN, I-10125 Torino, Italy
⁷⁵Universita di Trieste, Dipartimento di Fisica and INFN, I-34127 Trieste, Italy
⁷⁶Vanderbilt University, Nashville, TN 37235, USA
⁷⁷University of Victoria, Victoria, BC, Canada V8W 3P6
⁷⁸University of Wisconsin, Madison, WI 53706, USA
⁷⁹Yale University, New Haven, CT 06511, USA

(Dated: February 8, 2020)

We present a search for B decays to charm less final states involving charged or neutral a_0 mesons. The data sample corresponds to 89 million $B\bar{B}$ pairs collected with the BABAR detector operating at the PEP-II asymmetric-energy B Factory at SLAC. We find no significant signals and determine the following 90% C.L. upper limits: $B(B^0 \rightarrow a_0^+ \pi^-) < 5.1 \cdot 10^{-6}$, $B(B^0 \rightarrow a_0^- K^+) < 2.1 \cdot 10^{-6}$, $B(B^0 \rightarrow a_0^- K^0) < 3.9 \cdot 10^{-6}$, $B(B^+ \rightarrow a_0^0 \pi^+) < 5.8 \cdot 10^{-6}$, $B(B^+ \rightarrow a_0^0 K^+) < 2.5 \cdot 10^{-6}$, and $B(B^0 \rightarrow a_0^0 K^0) < 7.8 \cdot 10^{-6}$, where in all cases B indicates the product of branching fractions for $B \rightarrow a_0 X$ and $a_0 \rightarrow \pi^+$, where X indicates K or π .

PACS numbers: 13.25.Hw, 12.15.Hh, 11.30.Er

We report results on measurements of B -meson decays to charm less final states with $a_0(980)$ mesons [1]. Both experimentally and theoretically, most work in charm-less two-body B decays has involved states with only pseudoscalar and vector mesons. The only charm less B decay involving scalar mesons that has been observed is $B \rightarrow f_0(980)K$ [2]. There have been no previously published searches for B decays to final states with a_0 mesons. In this paper we search for the decays $B \rightarrow a_0^-$, $B \rightarrow a_0^- K$, and $B \rightarrow a_0^- K^0$ for both charged and neutral a_0 mesons. These measurements should provide information both for B decays to scalar mesons and the nature of those mesons.

Some specific predictions can be made for the decays $B \rightarrow a_0^-$ if factorization is assumed and if the decay is a "tree" process, that is, one in which a virtual W decays rather than being reabsorbed, as it is in a penguin (loop) process. The dominant such process is shown in Fig. 1(a). The companion tree process, shown in Fig. 1(b), is expected to be greatly suppressed, since the virtual W cannot produce an a_0 meson [4]. This is a prediction of the Standard Model because the weak current has a G-parity even vector part and a G-parity odd axial-vector part. The latter can produce an axial-vector or pseudoscalar particle while the former produces a vector particle, but neither can produce a G-parity odd scalar meson. Penguin processes such as shown in Fig. 1(c) are allowed, but are suppressed relative to the tree processes. Thus the decay $B \rightarrow a_0^-$ is expected to be "selftagging" (the charge of the pion identifies the B flavor). The decays with a kaon in the final state should be dominated by penguin processes (Fig. 1d); however, there is a cancellation for these decays [5], so they also should have rather small branching fractions. The diagrams for neutral B decays involving a_0^0 mesons are similar to those shown in Fig. 1.

The nature of the a_0 is still not well understood. It is thought to be a $q\bar{q}$ state with a possible admixture of a $K\bar{K}$ bound-state component due to the proximity to the $K\bar{K}$ threshold [6, 7]. The a_0 mass is known to be about 985 MeV and the dominant decay mode is $a_0 \rightarrow K^+ K^-$ [6], which is the mode used in the present analysis. A recent analysis [8] that uses this decay channel finds a Breit-Wigner width of (71 ± 7) MeV, with no better fit obtained when the more correct F latte shape [9] is used. Also since the branching fraction for $a_0 \rightarrow \pi^+ \pi^-$ is

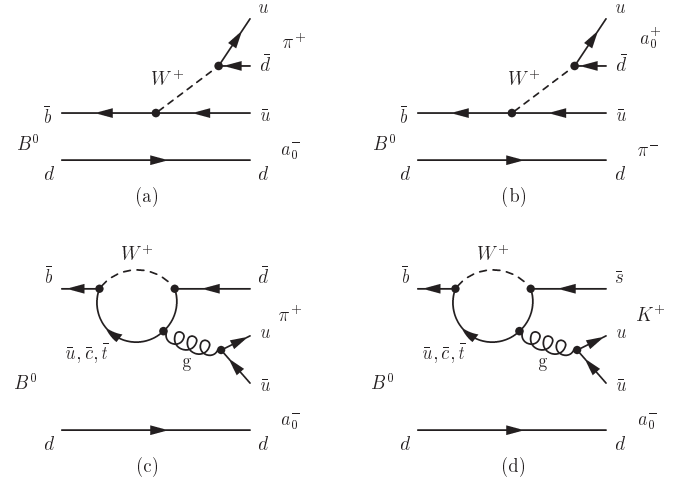


FIG. 1: Feynman diagrams for decays involving charged a_0 mesons: (a) dominant and (b) G-parity-suppressed tree diagrams for $B^0 \rightarrow a_0^-$, (c) penguin diagram for the same decay mode, and (d) penguin diagram for the decay $B^0 \rightarrow a_0^- K^+$.

not well known, we report the product branching fraction $B(B \rightarrow a_0 X) \cdot B(a_0 \rightarrow \pi^+ \pi^-)$, where X indicates K or π .

The results presented here are based on data collected with the BABAR detector [10] at the PEP-II asymmetric $e^+ e^-$ collider located at the Stanford Linear Accelerator Center. An integrated luminosity of 81.9 fb^{-1} , corresponding to 88.9 1.0 million $B\bar{B}$ pairs, was recorded at the $(4S)$ resonance (center-of-mass energy $\sqrt{s} = 10.58 \text{ GeV}$).

The track parameters of charged particles are measured by a combination of a silicon vertex tracker, with five layers of double-sided silicon sensors, and a 40-layer central drift chamber, both operating in the 1.5-T magnetic field of a superconducting solenoid. We identify photons and electrons using a CsI(Tl) electromagnetic calorimeter (EMC). Further charged particle identification (PID) is provided by the average energy loss (dE/dx) in the tracking devices and by an internally reflecting, ring-imaging Cherenkov detector (DIRC) covering the central region.

We select a_0 candidates from the decay channel $a_0 \rightarrow \pi^+ \pi^-$ with the decays $\pi^+ \rightarrow (\pi^+ \pi^-)$ and $\pi^- \rightarrow (\pi^+ \pi^-)$. We apply the following requirements on the in-

variant masses (in MeV) relevant here: $500 < m < 585$ for a_0 , $535 < m < 560$ for χ_1^0 , $120 < m < 150$ for χ_0^0 , and $775 < m < 1175$ for a_0^\pm . These requirements are typically quite loose compared with typical resolutions in order to achieve high efficiency and retain sufficient sidebands to characterize the background for subsequent fitting. We reconstruct K_s^0 candidates through the $K_s^0 \rightarrow \pi^+ \pi^-$ decay; to obtain a low-background, well-understood K_s^0 sample, we require $488 < m < 508$ MeV, the three-dimensional light distance from the event primary vertex to be greater than 2 mm, and the angle between light and momentum vectors, in the plane perpendicular to the beam direction, to be less than 40 mrad.

We make several PID requirements to ensure the identity of the pions and kaons. Secondary tracks in χ_1^0 candidates must have measured DIRC, $dE = dx$, and EMC outputs consistent with pions. For the decays $B \rightarrow a_0 h^+$ [3], where h^+ indicates a charged pion or kaon, the particle h^+ must have an associated DIRC signal with a Cherenkov angle within 3.5 standard deviations of the expected value for either a π or K hypothesis (we describe below the separation between the two hypotheses).

A B^- meson candidate is characterized kinematically by the energy-substituted mass $m_{ES} = [(\frac{1}{2}s + p_0 \cdot \vec{B})^2 - p_0^2]^{1/2}$ and energy difference $E = E_B - \frac{1}{2}\vec{s}$, where $(E_B; \vec{p}_B)$ and $(E_0; \vec{p}_0)$ are the four vectors of the B^- -candidate and the initial electron-positron system, respectively. The asterisk denotes the (4S) frame, and s is the square of the invariant mass of the electron-positron system. The $E(m_{ES})$ resolution is about 40 MeV (3.0 MeV). We require $|E_j| > 0.2$ GeV and $5.2 < m_{ES} < 5.29$ GeV.

Backgrounds arise primarily from random combinations in continuum $e^+ e^- \rightarrow q\bar{q}$ ($q = u; d; s; c$) events. We reduce these by using the angle τ between the thrust axis of the B^- candidate in the (4S) frame and that of the rest of the charged tracks and neutral clusters in the event. The distribution of $\cos \tau$ is sharply peaked near 1.0 for combinations drawn from jet-like $q\bar{q}$ pairs, and nearly uniform for B^- -meson decays. We require $|\cos \tau| < 0.9$ for the $a_0 K_s^0$ decay modes, tightening for higher-background $a_0 h^+$ channels: 0.8 for $a_0 (\chi_1^0) h^+$, 0.7 for $a_0 (\chi_0^0) h^+$ and $a_0^\pm (\chi_1^0) h^+$, and 0.6 for $a_0^\pm (\chi_0^0) h^+$. We also use, in the fit described below, a Fisher discriminant F that combines the angles with respect to the beam axis of the B^- momentum and B^- thrust axis (in the (4S) frame), and moments describing the energy flow about the B^- thrust axis [11].

For the a_0^\pm modes we use additional event-selection criteria to reduce backgrounds from several charmless B^- decay modes. We require $|\cos \theta_{dec}| < 0.86$, where θ_{dec} is the decay angle, the angle of the photons in the rest frame with respect to the boost direction from the B^- to that frame. We also require $\cos \theta_{dec}^a < 0.8$, where θ_{dec}^a is the a_0^\pm decay angle, defined similarly to θ_{dec} ,

with sign such that high-momentum mesons populate the region near +1. From Monte Carlo (MC) simulation [12] we estimate that the residual charmless $B\bar{B}$ background is less than one event for all decays except $a_0^\pm \rightarrow \pi^\pm \bar{K}^0$ (the notation indicates the decay mode of the used in reconstructing the a_0^\pm) and $a_0^\pm \rightarrow \pi^\pm h^+$, where we include in the total $B\bar{B}$ component, that we find to be less than 0.5% of the total sample in both cases.

We obtain yields and branching fractions from extended unbinned maximum likelihood fits, with input observables E , m_{ES} , F , m_τ , and for charged modes the PID variables S and S_K ; the last quantities are the number of standard deviations between the measured Cherenkov angle and the expectation for pions and kaons.

For each event i , hypothesis j (signal, continuum background, $B\bar{B}$ background), and, for the $a_0 h^+$ decays, flavor k , we define the probability density function (PDF)

$$P_{jk}^i = P_j(m_{ES}^i) P_j(E_k^i | S_k^i) P_j(F^i) P_j(m_i^i); \quad (1)$$

The term in brackets for S pertains to the $a_0 h^+$ modes. The absence of correlations among observables (except between E and S , which both depend on the momentum of the particle h^+) in the background P_{jk}^i , is confirmed in the (background-dominated) data samples entering the fit. For the signal component, we correct for effects due to the neglect of small correlations (more details are provided in the systematics discussion below). The likelihood function is

$$L = \exp \left(\sum_{j,k} \frac{Y_{jk}}{N} \right)^2 \prod_{j,k} Y_{jk} P_{jk}^i; \quad (2)$$

where Y_{jk} is the yield of events of hypothesis j and flavor k that we find by maximizing L , and N is the number of events in the sample.

We determine the PDF parameters from simulation for the signal and $B\bar{B}$ background components, and initial values of the continuum background parameters from (m_{ES}, E) sideband data. We parameterize each of the functions $P_{sig}(m_{ES})$; $P_{sig}(E_k)$; $P_j(F)$; $P_j(S_k)$ and the peaking component of $P_j(m_\tau)$ with either a Gaussian function, the sum of two Gaussian functions or an asymmetric Gaussian function, as required to describe the distribution. Slowly varying distributions (a_0 candidate mass and E for combinatoric background) are represented by second order Chebyshev polynomials. The $q\bar{q}$ combinatoric background in m_{ES} is described by the function $f(x) = x^{-1} x^2 \exp(-1/x^2)$, with $x = 2m_{ES}/\vec{p}_T^2$ and free parameter σ ; for $B\bar{B}$ background, we add a Gaussian function to the quantity $f(x)$. Large control samples of $B^- D^-$ decays of topology similar to the signal are used to verify the simulated resolutions in E and m_{ES} . Where the control data samples reveal differences from MC, we shift or scale the resolution used

in the likelihood fits. Examples of many of these PDF shapes from a very similar analysis are shown in Ref. [11]. Additionally, the Breit-Wigner signal parameters for the a_0 mass and width are determined from an inclusive dataset that is much larger than the sample used for this analysis. The widths are consistent with expectations from the natural-width values of Ref. [8].

In Table I we show for each decay mode the measured product branching fraction, together with the quantities entering into its determination. The free parameters in the fit include the signal and background yields and six parameters describing the background PDFs: slopes for the polynomial shape for the E and a_0 mass distributions, the parameter used in the m_{ES} description, and three parameters describing the asymmetric Gaussian function for F . For calculation of branching fractions, we assume that the decay rates of the (4S) to B^+B^- and $B^0\bar{B}^0$ are equal [13]. We combine branching fraction results from the two decay channels by adding the values of $2 \ln L$, adjusted for a small bias (see below) and taking proper account of the correlated and uncorrelated systematic errors. In Figs. 2 and 3 we show projections onto m_{ES} and E of subsamples enriched with mode-dependent threshold requirement on the signal likelihood (computed ignoring the PDF associated with the variable plotted).

The statistical error on the signal yield is taken as the change in the central value when the quantity $2 \ln L$ increases by one unit from its minimum value. The significance is taken as the square root of the difference between the value of $2 \ln L$ (with systematic uncertainties included) for zero signal and the value at the minimum, with other parameters free in both cases. The 90% confidence level (C.L.) upper limit is taken to be the branching fraction below which lies 90% of the total of the likelihood integral in the positive branching fraction region.

Most of the yield uncertainties arising from lack of knowledge of the PDFs have been included in the statistical error since most background parameters are free in the fit. Varying the signal PDF parameters within their estimated uncertainties, we determine the uncertainties in the signal PDFs to be 1–5 events, depending on the final state. The contribution to this uncertainty from the parameterization of the a_0 signal shape is small. We verify that the value of the likelihood of each fit is consistent with the expectation found from an ensemble of simulated experiments.

Uncertainties in our knowledge of the efficiency, found from auxiliary studies, include 0.8% N_t , 2.5% N_γ , and 4% for a K_s^0 decay, where N_t and N_γ are the number of signal tracks and photons, respectively. Our estimate of the number of produced $B\bar{B}$ events is uncertain by 1.1%. The neglect of correlations among observables in the fit can cause a systematic bias; the correction for this bias (between –3 and +3 events) and assignment of the resulting systematic uncertainty (0.5–2 events) is deter-

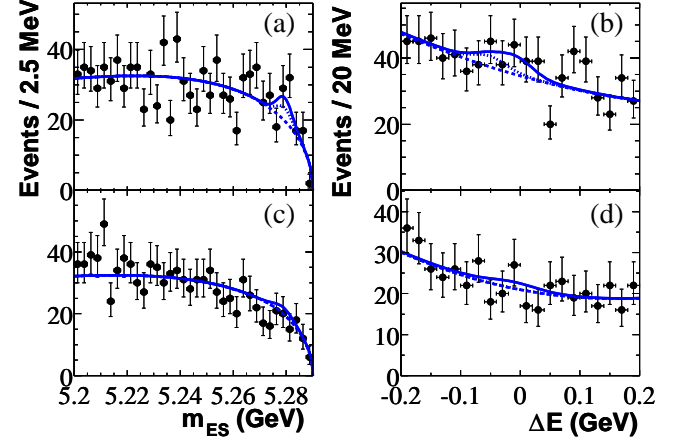


FIG. 2: Projections of the B -candidate m_{ES} and E for (a, b) $a_0 h^+$, and (c, d) $a_0^0 h^+$. Points with errors represent data, solid curves the full t functions, dashed curves the background functions (the peaking $B\bar{B}$ background component is negligible), and the dotted curve shows the kaon portion of the signal. These plots are made with a minimum requirement on the likelihood and thus do not show all events in the data samples.

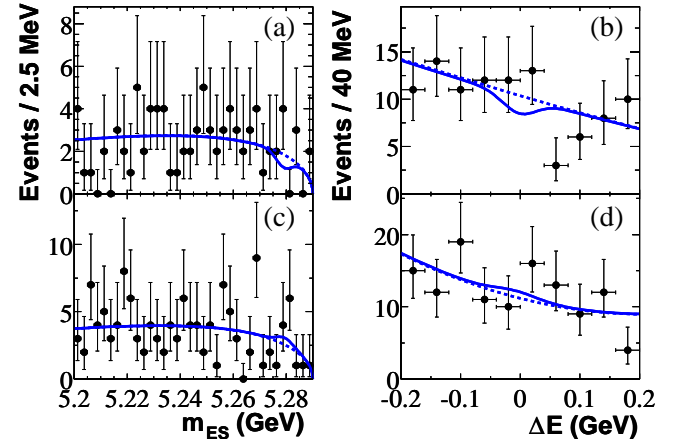


FIG. 3: Projections of the B -candidate m_{ES} and E for (a, b) $a_0 K_s^0$, and (c, d) $a_0^0 K_s^0$. Points with errors represent data, solid curves the full t functions, and dashed curves the background functions. These plots are made with a minimum requirement on the likelihood and thus do not show all events in the data samples.

mined from simulated samples with varying background populations. Published data [6] provide the uncertainties in the B -daughter product branching fractions (1–2%). Selection efficiencies uncertainties are 0.5(3.5%) for $\cos \theta_T$ and 0.5% for PID (for the $a_0 h^+$ modes).

In conclusion, we do not find significant signals for these B -meson decays to states with a_0 mesons. The measured branching fractions and 90% C.L. upper limits

TABLE I: Signal yield, detection efficiency, daughter branching fraction product (\bar{B}_i), significance (including systematic uncertainties, taken to be zero if corrected yield is negative), measured product branching fraction (see text), and the 90% C.L. upper limit on this branching fraction.

M mode	Yield (%)	\bar{Q}	\bar{B}_i (%)	Signif.	$B(10^{-6})$	UL (10^{-6})
$a_0^0 (\cdot \cdot \cdot)^+$	18^{+11}_{-10}	18.8	39.4	1.3	$2.3^{+1.7}_{-1.5}$	0.9
$a_0^0 (\cdot \cdot \cdot)^+$	15^{+9}_{-8}	15.5	22.6	1.6	$3.9^{+2.9}_{-2.5}$	1.0
$a_0^0 (\cdot \cdot \cdot)^+$				2.0	$2.8^{+1.5}_{-1.3}$	< 5.1
$a_0^0 (\cdot \cdot \cdot)K^+$	2^{+6}_{-4}	17.9	39.4	0.1	$0.0^{+0.9}_{-0.6}$	0.3
$a_0^0 (\cdot \cdot \cdot)K^+$	13^{+8}_{-6}	14.9	22.6	1.1	$3.1^{+2.5}_{-2.1}$	1.9
$a_0^0 K^+$				0.4	$0.4^{+1.0}_{-0.8}$	0.2
$a_0^0 (\cdot \cdot \cdot)\bar{K}^0$	12^{+8}_{-6}	21.4	13.5	0.0	$3.7^{+2.9}_{-2.3}$	0.9
$a_0^0 (\cdot \cdot \cdot)\bar{K}^0$	0^{+7}_{-5}	15.8	7.9	0.5	$2.7^{+6.1}_{-4.4}$	1.9
$a_0^0 \bar{K}^0$				0.6	$1.5^{+2.4}_{-1.8}$	< 3.9
$a_0^0 (\cdot \cdot \cdot)^+$	17^{+11}_{-9}	12.8	39.4	1.4	$3.1^{+2.4}_{-2.0}$	1.2
$a_0^0 (\cdot \cdot \cdot)^+$	1^{+8}_{-6}	9.5	22.6	0.3	$1.2^{+3.9}_{-3.2}$	1.7
$a_0^0 (\cdot \cdot \cdot)^+$				1.4	$2.6^{+2.0}_{-1.7}$	< 5.8
$a_0^0 (\cdot \cdot \cdot)K^+$	0^{+5}_{-3}	12.4	39.4	0.3	$0.3^{+1.1}_{-0.6}$	0.4
$a_0^0 (\cdot \cdot \cdot)K^+$	6^{+7}_{-5}	9.1	22.6	0.5	$1.9^{+3.8}_{-2.9}$	2.5
$a_0^0 K^+$				0.4	$0.4^{+1.1}_{-0.7}$	< 2.5
$a_0^0 (\cdot \cdot \cdot)K^0$	0^{+6}_{-5}	15.0	13.3	0.5	$1.4^{+3.5}_{-2.4}$	1.2
$a_0^0 (\cdot \cdot \cdot)K^0$	4^{+5}_{-4}	9.7	7.8	1.2	$6.6^{+5.4}_{-5.4}$	2.8
$a_0^0 K^0$				1.0	$2.8^{+3.1}_{-2.4}$	< 7.8

are given in Table I. Assuming to be the dominant mode, we rule out the predictions for the decay $B \rightarrow a_0 \bar{K}^0$ derived in Ref. [14].

We are grateful for the excellent luminosity and machine conditions provided by our PEP-II colleagues, and for the substantial dedicated effort from the computing organizations that support BABAR. The collaborating institutions wish to thank SLAC for its support and kind hospitality. This work is supported by DOE and NSF (USA), NSERC (Canada), IHEP (China), CEA and CNRS-IN2P3 (France), BMF and DFG (Germany), INFN (Italy), FOM (The Netherlands), NFR (Norway), MIST (Russia), and PPARC (United Kingdom). Individuals have received support from CONACYT (Mexico), A.P.Sloan Foundation, Research Corporation, and Alexander von Humboldt Foundation.

- [1] Throughout this note, when we refer to a_0 , we mean specifically $a_0(980)$.
- [2] Belle Collaboration, A.Garmash et al., Phys. Rev. D 65, 092005 (2002); BABAR Collaboration, B.Aubert et al., hep-ex/0308065 (submitted to Phys. Rev. D), 2003; BABAR Collaboration, B.Aubert et al., hep-ex/0406040 (submitted to Phys. Rev. Lett.), 2004.
- [3] The named member of a charge-conjugate pair of particles stands for either.
- [4] S. Laplace and V. Shelkov, Eur. Phys. Jour. C 22, 431 (2001).
- [5] V. Chemyak, Phys. Lett. B 509, 273 (2001).
- [6] Particle Data Group, K. Hagiwara et al., Phys. Rev. D 66, 010001 (2002).
- [7] V. Baru et al., Phys. Lett. B 586, 53 (2004).
- [8] S. Teige et al., Phys. Rev. D 59, 012001 (1998).
- [9] S. Flatté, Phys. Lett. B 63, 224 (1976).
- [10] BABAR Collaboration, B. Aubert et al., Nucl. Instr. Meth. A 479, 1 (2002).
- [11] BABAR Collaboration, B. Aubert et al., hep-ex/0403025 (2004).
- [12] The BABAR detector Monte Carlo simulation is based on GEANT4: S. Agostinelli et al., Nucl. Instr. Meth. A 506, 250 (2003).
- [13] See for instance BABAR Collaboration, B. Aubert et al., Phys. Rev. D 69, 071101 (2004) and references therein.
- [14] P. Minkowski and W. Ochs, hep-ph/0404194 (2004).

Now at Department of Physics, University of Warwick, Coventry, United Kingdom.

^y Also with Università della Basilicata, Potenza, Italy

^z Also with IFIC, Instituto de Física Corpuscular, CSIC-Universidad de Valencia, Valencia, Spain

^x Deceased